



Photochemical and Sono-Photochemical Studies of Zn (II) Porphyrin-conjugated Chitosan Hydrogels for Enhanced Singlet Oxygen Generation

Artırılmış Singlet Oksijen Üretimi İçin Zn (II) Porfirin-Konjuge Kitosan Hidrojellerinin Fotokimyasal ve Sono-Fotokimyasal İncelemeleri

Emel Önal[✉]

Faculty of Engineering, Doğu University, İstanbul, Türkiye.

ABSTRACT

This study investigates the synthesis, characterization, and photochemical properties of porphyrin-chitosan hydrogels. These hydrogels, developed for potential use in photodynamic therapy (PDT) and sono-photodynamic therapy (SPDT), efficiently produce singlet oxygen, an essential reactive oxygen species (ROS) for therapy. Zinc (II) porphyrins 1 and 2 were synthesized by metal insertion to free based porphyrins and covalently linked to chitosan via Schiff-base reaction to produce chitosan hydrogel CS-1 and CS-2 (conjugation via phenylacetylene spacer). Spectroscopic analysis confirmed successful conjugation of the porphyrins, with SEM imaging showing an even distribution of porphyrins within the hydrogel. Photophysical and photochemical properties, including ground state absorption and singlet oxygen generation, were evaluated for both porphyrin complexes and chitosan-conjugated hydrogels in DMSO. The porphyrin-hydrogel structures showed superior singlet oxygen generation efficiency. Sono-photochemical studies showed further enhanced singlet oxygen generation, with the highest quantum yield ($\Phi_{\Delta} = 0.81$) observed for the chitosan hydrogel CS-2. The results demonstrated enhanced singlet oxygen generation in the hydrogel structures, particularly under simultaneous ultrasound and light irradiation, indicating their potential efficacy in PDT and SPDT applications. Additionally, photo degradation studies revealed the stability of the synthesized compounds under light irradiation. These findings highlight the potential of porphyrin-conjugated chitosan hydrogels as effective photosensitizers for PDT and SPDT applications.

Key Words

Zn (II) Porphyrin, chitosan, hydrogel, singlet oxygen generation, photodynamic therapy (PDT), sono-photodynamic therapy (SPDT).

Öz

Bu çalışmada porfirin-kitosan hidrojellerinin sentezi, karakterizasyonu ve fotokimyasal özellikleri incelenmiştir. Fotodinamik terapi (PDT) ve sono-fotodinamik terapide (SPDT) potansiyel kullanım için geliştirilen bu hidrojeller, terapi için gerekli bir reaktif oksijen türü (ROS) olan singlet oksijeni verimli bir şekilde üretir. 1 ve 2 numaralı Zn (II) porfirinler, metallsiz porfirinlere metal eklenmesi yoluyla sentezlenmiş ve CS-1 ve CS-2 numaralı kitosan hidrojelleri üretmek için Schiff-baz reaksiyonu yoluyla (fenilasetilen yoluyla konjugasyon) kitosana kovalent olarak bağlanmıştır. Spektroskopik analizler, porfirinlerin başarılı bir şekilde konjugasyonunu doğrulamış ve SEM görüntülemesi, porfirinlerin hidrojel içinde eşit bir şekilde dağıldığını göstermiştir. DMSO içinde hem porfirin kompleksleri hem de kitosan-konjuge hidrojeller için temel hal absorpsiyonu ve singlet oksijen üretimi dahil olmak üzere fotofiziksel ve fotokimyasal özellikler değerlendirilmiştir. Porfirin-hidrojel yapıları üstün singlet oksijen üretim etkinliği göstermiştir. Sono-fotokimyasal çalışmalar, kitosan hidrojel CS-2 için gözlemlenen en yüksek kuantum verimi ($\Phi_{\Delta} = 0.81$) ile singlet oksijen üretiminin daha da arttığını göstermiştir. Elde edilen sonuçlar, hidrojel yapılarında, özellikle eşzamanlı ultrasound ve ışık ile uyarılma altında, PDT ve SPDT uygulamalarında potansiyel etkinliklerini gösteren gelişmiş singlet oksijen üretimi olduğunu göstermiştir. Ayrıca, foto bozunma çalışmaları sentezlenen bileşiklerin ışık ile uyarılma altında kararlılığını ortaya koymuştur. Bu bulgular, porfirin konjuge kitosan hidrojellerinin PDT ve SPDT uygulamaları için etkili fotosensitizerler olarak potansiyelini vurgulamaktadır.

Anahtar Kelimeler

Zn (II) Porfirin, kitosan, hidrojel, singlet oksijen üretimi, fotodinamik terapi (PDT), sono-fotodinamik terapi (SPDT).

Article History: May 31, 2024; Accepted: Nov 28, 2024; Available Online: Dec 18, 2024.

DOI: <https://doi.org/10.15671/hjbc.1492613>

Correspondence to: E. Önal, Faculty of Engineering, Doğu University, İstanbul, Türkiye.

E-Mail: eonal@dogus.edu.tr

INTRODUCTION

In cancer treatment, new methods like photodynamic therapy (PDT) [1], sonodynamic therapy (SDT) [2,3], and sono-photodynamic therapy (SPDT) [4] aim to precisely target cancer cells while sparing healthy tissues. Each method offers unique benefits and limitations. The efficient production of singlet oxygen, a highly reactive and cytotoxic ROS species, is crucial for the success of these treatments. Therefore, the choice of a suitable photosensitizer is essential, requiring key features such as high stability, low toxicity, optimal absorption characteristics, biocompatibility, and solubility.

Extensive research has focused on utilizing porphyrins as photosensitizing agents, emphasizing their ability to generate singlet oxygen [5], their fluorescence characteristics, and their stability [6]. Over the past decade, there has been a significant interest in the exploration and utilization of porphyrins, with a growing emphasis on investigating porphyrin bio-molecular-based systems including porphyrin-based nanomedicines [7], metal-organic framework compounds [8], and polymeric micelles [9,10]. This is driven by the advantageous preferential targeting localization of porphyrins in tumours, coupled with their capacity to generate reactive singlet oxygen and exhibit low dark toxicities. This dual emphasis highlights the multifaceted potential of porphyrins, advancing not only the field of photodynamic therapy but also contributing to the development of innovative biomedical applications such as multimodal cancer photodynamic therapy [11], drug delivery systems [12], and nanotheranostics [13].

To further optimize porphyrins for these applications, modifications with ethynyl groups at specific positions, like the *meso* or β -position, have proven effective [14]. Ethynyl groups, known for their electron-donating properties and coplanarity, extend the π -conjugation in porphyrins, leading to red shifts in absorption and emission spectra. This spectral shift enhances their singlet oxygen generation capacity under light, a critical aspect of PDT [15], allowing deeper tissue penetration with near-IR light [16]. Thus, the strategic inclusion of ethynyl linkers fine-tunes porphyrins' optical properties for various biomedical and optoelectronic uses.

Further advancements address the inherent water insolubility of porphyrins. To overcome this, current research efforts have shifted towards developing porphyrin-nanomaterial conjugated systems as a viable solution for overcoming this obstacle.

Chitosan is a natural cationic biopolymer composed of β -(1,4)-linked D-glucosamine and N-Acetyl-D-glucosamine (Scheme 1). Thanks to its biocompatible, biodegradable polymer structure and unique properties, it has garnered significant attention in the field of biomedical drug delivery [17-20] and photodynamic therapy (PDT) [21-22]. In recent years, there has been a growing interest in the development and application of chitosan-conjugated porphyrins for PDT [23]. The combination of chitosan with porphyrin-based photosensitizers has shown promise in targeted PDT including cancer [24] and microbial infections [25], offering enhanced singlet oxygen generation [26], improved biocompatibility, and pH stability [27]. This comprehensive approach underscores the potential of chitosan-conjugated porphyrins as a versatile and effective strategy in the realm of therapeutic methods.

In this context, the objective of this study was to synthesize new Zn (II) porphyrins and covalently conjugate them with chitosan hydrogels to assess their photochemical and sono-photochemical properties.

Experimental

Materials and Instruments

1,3-Diphenylisobenzofuran (DPBF), zinc (II) acetate dihydrate ($\text{Zn}(\text{OAc})_2 \cdot 2\text{H}_2\text{O}$), dimethyl formamide (DMF), tetrahydrofuran (THF), NaOH, dimethyl sulfoxide (DMSO), chitosan (Low molecular weight) was purchased from Sigma Aldrich and Merck. Unless otherwise specified, reagents and solvents were of commercial quality and were used without further purification. Preparative separations were performed by silica gel column chromatography Merck-60 (43–63 mesh) and TLC on aluminium sheets precoated with silica gel 60F₂₅₄ (Merck). Infrared spectra were measured on a Perkin Elmer Spectrum 100 FT-IR spectrometer in transmittance mode with an attenuated total reflection (ATR) accessory featuring a zinc selenide (ZnSe) crystal. A film section of about 1 cm² was cut to be analysed. Spectra were recorded at 1.0 cm⁻¹ resolution, in the range 4000–400 cm⁻¹ as a ratio of 64 single-beam scans of the sample to the same number of background scans from air. ¹H NMR spectra were recorded on an Agilent 500 MHz spectrometer using TMS as the internal reference. The mass spectra were recorded on MALDI (matrix-as-

sisted laser desorption ionization) BRUKER Microflex LT using 2,5-dihydroxybenzoic acid as matrix. Absorption spectra in the UV-visible region was recorded with a Sinco S-3100 UV-vis spectrophotometer using a 1 cm path length quartz cuvette between a maximum range of 300 and 1100 nm. Solutions were freshly prepared in spectrophotometric grade solvents. Molar extinction coefficients (ϵ) were determined by measurement of the absorption solutions of differing concentrations for each compound, followed by determination of the slope. Photo irradiations were measured using a General Electric quartz line lamp (300W). A 600 nm glass cut-off filter (Schott) and a water filter were used to filter off ultraviolet and infrared radiations respectively. An interference filter (Intor, 400 nm with a bandwidth of 70 nm) was additionally placed in the light path before the sample. Wisd Ultrasonic WUC-A22 H was used for ultrasound irradiation. The images of porphyrin-conjugated chitosan hydrogel were taken with Scanning Electron Microscopy (SEM), JEOL JCM-6000Plus.

Synthesis of porphyrin 1 and 2

In our previous paper, free-based porphyrins 5-(4-formylphenyl)-10,15,20-tris (4-(hexyloxyphenyl) porphyrin and 5-(4-formylphenylethynyl)-10,15,20-tris (4-(hexyloxyphenyl) porphyrin were synthesized and characterized [28]. For Zinc (II) metal insertion, to a stirred solution of 9.5 μmol free porphyrins in dry DMF (4 mL), 14.25 μmol of dry Zn (OAc)₂ (2.6 mg, 1.5 eqv.) was added. The reaction mixture was heated to reflux (153 °C) and stirred for 24 h under an argon atmosphere. The resulting reaction mixture was poured into water (100 mL) to give precipitates which were then filtered and further washed with water. Purification by column chromatography (SiO₂, CH₂Cl₂:C₆H₁₄ (5:1)) gave the target porphyrin 1 (6.6 mg, 6.65 μmol) in 70 % yield, and porphyrin 2 (6 mg, 5.7 μmol) in 60 % yield as dark purple color solids.

Porphyrin 1. FT-IR, ν (cm⁻¹): 2956, 2923 (CH_{Ar}), 2856 (CH_{aliphatic}), 1723 (C = O), 1493 (C = C_{phenyl}), 1461 (C = N), 1185, (CH_{pyrrole}), 959 (CH_{porph. Ring}), 730 (CH_{pyr. Ring}). MS-MALDI-TOF (m/z) C₆₃H₆₄N₄O₄Zn [calcd]: 1004.42, [found]: 1004.16 [M]⁺.

¹H NMR (500 MHz, CDCl₃) δ (ppm): 1.02 (s, 9H, methyl-H), 1.46, 1.52 (b, 12H, CH₂ (8,9)), 1.64 (m, 6H, CH₂ (7)), 1.98 (m, 6H, CH₂(6)), 4.26 (t, J = 6.3 Hz, 6H, CH₂(5)), 7.29 (d, J = 6.1 Hz, 6H, CH (3)), 8.11 (d, J = 8.3 Hz, 6H, CH (4)), 8.31 (d, J

= 7.8 Hz, 2H, CH (2)), 8.41(d, J = 7.6 Hz, 2H, CH (1)), 8.90 (m, 6H, CH (pyrrole)), 10.41 (s, 1H, CHO). ¹³C NMR (125 MHz, CDCl₃); δ ppm: 163.30 (CHO), 156.21-124.81 (Ar-CH), 59.52 (OCH₂), 30.15-22.15 (CH₂), 14.12 (CH₃). UV-vis (λ , nm) (DMSO) 432 (5.01), 564 (3.83), 607 (3.74).

Porphyrin 2. FT-IR ν (cm⁻¹): 2955, 2921 (CH_{Ar}), 2852 (CH_{aliphatic}), 2212 (C \equiv C), 1723 (C = O), 1464 (C = N), 1173 (C-H_{pyrrole}), 995 (C-H_{porp. ring}), 795 (C-H_{pyr. ring}). MS-MALDI-TOF (m/z) C₇₁H₆₈N₄O₄Zn [calcd]: 1104.45, [found]: 1104.18 [M]⁺. ¹H NMR (500 MHz, CDCl₃) δ (ppm): 0.95 (s, 9H, methyl-H), 1.02, 1.55 (b, 12H, CH₂ (8,9)), 1.66 (m, 6H, CH₂ (7)), 1.92 (m, 6H, CH₂(6)), 4.27 (t, J = 6.3 Hz, 6H, CH₂(5)), 7.29 (d, J = 7.1 Hz, 6H, CH (3)), 7.82 (d, J = 6.9 Hz, 2H, CH (β)), 7.97 (d, J = 6.3 Hz, 2H, CH (2)), 8.13(d, J = 4.4 Hz, 2H, CH (1)), 8.26(d, J = 6.3 Hz, 2H, CH (4)), 8.31(d, J = 6.9 Hz, 2H, CH(α)), 8.89 (m, 6H, CH (pyrrole)), 10.05 (s, 1H, CHO). ¹³C NMR (125 MHz, CDCl₃); δ ppm: 160.83 (CHO), 145.32-112.08 (Ar-CH), 68.27 (OCH₂), 31.12-22.32 (CH₂), 13.10 (CH₃). UV-vis (λ , nm) (DMSO) 432 (5.04), 565(3.89), 608(3.85).

Preparation of porphyrin-conjugated chitosan hydrogel CS-1 and CS-2

The conjugation of porphyrins to chitosan was accomplished through Schiff's base reaction between amino groups on chitosan and aldehyde groups on porphyrin termini. This procedure was carried out using previously reported methods with slight modifications[22, 29-32]. Briefly, to prepare 10 wt% chitosan conjugates, 5 mg of each porphyrin was dissolved in 2 mL of DMF and added drop by drop to a mixture of chitosan (50 mg) in 1% acetic acid (5 mL). The homogeneous was solution stirred at room temperature for 48 h. 2 M NaOH (5 mL) solution was poured into the reaction mixture, stirred for 6 hr, and stored in NaOH solution for 24 h then hydrogels were collected by centrifugation. Then, the hydrogels were rinsed repeatedly with excess distilled water until neutral pH.

CS-1. FT-IR ν (cm⁻¹): 3355 (NH_{2chitosan}), 3310 (OH_{chitosan}), 2915, 2884 (CH_{Ar}), 1649 (C=N), 1579 (N-H_{chitosan bending}), 1150 (C-H_{pyrrole}), 1060 (-C-O-C_{chitosan}) 1026 (-C-O-H_{chitosan}), 895(C-H_{chitosan β glycosidic bond}). UV-vis (λ , nm) (DMSO) 432(4.95), 566(4.26), 609(4.22).

CS-2. FT-IR ν (cm⁻¹): 3365 (NH_{2chitosan}), 3305 (OH_{chitosan}), 2923, 2872 (CH_{Ar}), 1644 (C=N), 1579 (N-H_{chitosan bending}), 1149 (C-H_{pyrrole}), 1060 (-C-O-C_{chitosan}) 1034 (-C-O-H_{chitosan}), 894(C-H_{chitosan β glycosidic bond}). UV-vis (λ , nm) (DMSO) 432(5.03), 566(4.39), 609(4.35).

Singlet oxygen quantum yield (Φ_{Δ}) determination

Singlet oxygen quantum yield (Φ_{Δ}) determinations were carried out a 2 mL portion of the CS-Por. solutions containing the singlet oxygen quencher irradiated in the Q band region with the photo-irradiation set-up described in the reference [33]. For singlet oxygen measurements, DPBF was used as a chemical quencher ($\Phi_{\Delta} \text{H}_2\text{TPP} = 0.52$ in DMSO) [34]. DPBF degradation at 417 nm was monitored by UV-Vis spectroscopy. The solutions of 10×10^{-6} M of complexes (1 mL) containing DPBF 1 mL ($\sim 1 \times 10^{-5}$ M) were prepared in the dark and irradiated in the Q band region. The light intensity of 7.05×10^{15} photons $\text{s}^{-1} \text{cm}^{-2}$ was used for Φ_{Δ} determinations. Singlet oxygen quantum yields (Φ_{Δ}) were calculated using equation 1. In the equation, R and R_{Std} were DPBF's photobleaching rates in the presence of the respective samples and standard, respectively, while I_{Abs} and $I_{\text{Abs}}^{\text{Std}}$ were the rates of light absorption by the samples and standard, respectively.

$$\Phi_{\Delta} = \Phi_{\Delta}^{\text{Std}} \frac{R \cdot I_{\text{Abs}}^{\text{Std}}}{R_{\text{Std}} \cdot I_{\text{Abs}}} \quad (1)$$

Photodegradation quantum yield (Φ_d) determination

Photodegradation quantum yields were determined using Eq. 2,

$$\Phi_d = \frac{(C_o - C_t) V \cdot N_A}{I_{\text{Abs}} \cdot S \cdot t} \quad (2)$$

where " C_o " and " C_t " are the sample concentrations before and after irradiation respectively, " V " is the reaction volume, " N_A " is the Avogadro's constant, " S " is the irradiated cell area, " t " is the irradiation time, " I_{Abs} " is the overlap integral of the radiation source light intensity and the absorption of the sample. A light intensity of 1.38×10^{16} photons $\text{s}^{-1} \text{cm}^{-2}$ was employed to determine the photodegradation. The degradation of max. Q band was monitored after each 10-minute irradiation.

Results and discussion

Synthesis and characterization

As shown in Scheme 1, a Schiff-base reaction was used to create a covalently cross-linked chitosan hydrogel

with porphyrin photosensitizers. Two structural variations were introduced in the porphyrin molecules: the addition of electron-donating hexyloxy chains at the *para* position of the *meso*-phenyl and the incorporation of a phenyl acetylide spacer between the porphyrin macrocycle and the chitosan. The hexyloxy chains are expected to improve the solubility of the dyads while also enhancing electron-donating effects on their photophysical properties. Meanwhile, the phenyl acetylide spacer introduces rigidity to the structure, extends π -conjugation, and increases luminescence. Phenyleneethynylene subunits serve as linking bridges[35,36], facilitating a high degree of conjugation between the donor (porphyrin), and the acceptor (chitosan).

The target porphyrins synthesized were Zinc porphyrin 1, with an aldehyde group directly attached to the *para* position of the *meso*-phenyl substituent, and porphyrin 2, featuring an aldehyde group separated from the porphyrin macrocycle by a phenyl acetylide spacer. These porphyrins were successfully obtained from their free-base derivatives, achieving reaction yields of 70% and 60%, respectively, as detailed in our previous study. [28]. The synthesizing procedure of porphyrin 1 and 2 is outlined in the experimental section. Chemical structures were characterized using standard tools such as Mass, FT-IR, ^1H NMR, ^{13}C NMR and UV-Vis spectroscopies (Figure 1-2 and Figure S1-S6).

In the FT-IR absorption spectra (Figures 1 and 2), peaks at 2956 and 2923 cm^{-1} for porphyrin 1 and at 2955 cm^{-1} and 2921 cm^{-1} for porphyrin 2 correspond to aromatic C-H stretching vibrations. Aliphatic C-H stretches appear at 2856 cm^{-1} for porphyrin 1 and at 2852 cm^{-1} for porphyrin 2. For porphyrin 2, a weak ethynyl ($\text{C}\equiv\text{C}$) vibration is detected at 2212 cm^{-1} . Both porphyrins exhibit strong aldehyde $\text{C}=\text{O}$ stretches around 1723 cm^{-1} . Additionally, characteristic vibrations of the porphyrin macrocycle[37,38] are seen at 1461 cm^{-1} ($\text{C}=\text{N}$) for porphyrin 1 and 1464 cm^{-1} for porphyrin 2. The porphyrin ring vibrations occur at 959 cm^{-1} and 995 cm^{-1} , while the peaks at 730 cm^{-1} and 795 cm^{-1} correspond to pyrrole ring bending. Lastly, pyrrole ring vibrations appear at 1185 cm^{-1} for compound 1 and 1173 cm^{-1} for compound 2.

The MALDI-TOF mass spectra of porphyrins 1 and 2 displayed peaks corresponding to their molecular ions $[\text{M}]^+$ (Figure S1 and S2). For porphyrin 1 ($\text{C}_{63}\text{H}_{64}\text{N}_4\text{O}_4\text{Zn}$), the calculated molecular weight is 1004.42 Da, and the experimental value observed was 1004.16 Da. For

porphyrin 2 ($C_{71}H_{68}N_4O_4Zn$), the calculated molecular weight is 1104.45 Da, with an experimental value of 1104.18 Da. The minimal differences between the calculated and observed masses (0.26 Da for 1 and 0.27 Da for 2) indicate excellent agreement, confirming the identity and integrity of the molecular ions for both compounds.

The 1H NMR spectra of compounds 1 and 2 (Figures S3-S4) were recorded, showing distinct signals for the porphyrin structures.

For porphyrin 1, the three aliphatic hexyloxy chains display signals for their CH_2 groups: a broad signal between 1.46 and 1.52 ppm (12H) corresponds to the CH_2 protons at positions 8 and 9, while a multiplet at 1.64 ppm accounts for the CH_2 protons at position 7 (6H). Another multiplet at 1.98 ppm is attributed to the CH_2 groups at position 6 (6H), and a triplet at 4.26 ppm ($J = 6.3$ Hz) represents the CH_2 groups directly attached to oxygen (6H). A singlet at 1.02 ppm corresponds to the methyl protons from the hexyloxy chains (9H). The aromatic region shows a doublet at 7.29 ppm ($J = 6.1$ Hz) from the protons on the phenyl rings at position 3 (6H) and a doublet at 8.11 ppm ($J = 8.3$ Hz) from the phenyl rings at position 4 (6H). The aromatic protons on the aldehyde-substituted phenyl ring are represented by two doublets at 8.31 ppm ($J = 7.8$ Hz, 2H) and 8.41 ppm ($J = 7.6$ Hz, 2H) for positions 2 and 1, respectively. A multiplet at 8.90 ppm corresponds to the protons on the pyrrole rings of the porphyrin core (6H), while a singlet at 10.41 ppm represents the aldehyde proton (1H) (Figure S3).

For porphyrin 2, the hexyloxy chain protons appear similarly: a singlet at 0.95 ppm for the methyl groups (9H), a broad signal between 1.02 and 1.55 ppm for the CH_2 groups at positions 8 and 9 (12H), a multiplet at 1.66 ppm for the CH_2 protons at position 7 (6H), and a multiplet at 1.92 ppm for the CH_2 groups at position 6 (6H). The CH_2 groups adjacent to oxygen show a triplet at 4.27 ppm ($J = 6.3$ Hz, 6H). The aromatic protons on the phenyl rings of the hexyloxy groups give rise to a doublet at 7.29 ppm ($J = 7.1$ Hz, 6H), while the β protons on the ethynyl linker appear as a doublet at 7.82 ppm ($J = 6.9$ Hz, 2H). A doublet at 7.97 ppm ($J = 6.3$ Hz) corresponds to the protons at position 2 on the formylphenyl ring (2H), and a doublet at 8.13 ppm ($J = 4.4$ Hz) represents the protons at position 1 (2H). Additionally, the protons on the phenyl rings at position 4 of the porphyrin

give a doublet at 8.26 ppm ($J = 6.3$ Hz, 2H), while the α protons on the ethynyl group show a doublet at 8.31 ppm ($J = 6.9$ Hz, 2H). The multiplet at 8.89 ppm is assigned to the pyrrole protons (6H), and the singlet at 10.05 ppm corresponds to the aldehyde proton on the formylphenylethynyl group (1H) (Figure S4).

In addition, to confirm the structures of porphyrins 1 and 2, the ^{13}C NMR spectra were recorded (Figures S5-S6). Methyl (CH_3) carbons appeared at 14.12 and 13.10 ppm for compounds 1 and 2, respectively. The aliphatic ethylene (CH_2) carbons resonated between 30.15–22.15 ppm for 1 and from 31.12–22.32 ppm for 2. The ethyl CH_2 carbons in the hexyl chain linked to oxygen (OCH_2) showed signals at 59.52 ppm and 98.27 ppm for 1 and 2, respectively. Aromatic (CH) carbons resonated between 156.21–124.81 ppm for 1 and from 145.32–112.08 ppm for 2, while aldehyde (CHO) carbons shifted to 163.30 ppm for 1 and 160.83 ppm for 2. These NMR findings align with the proposed structures of the compounds.

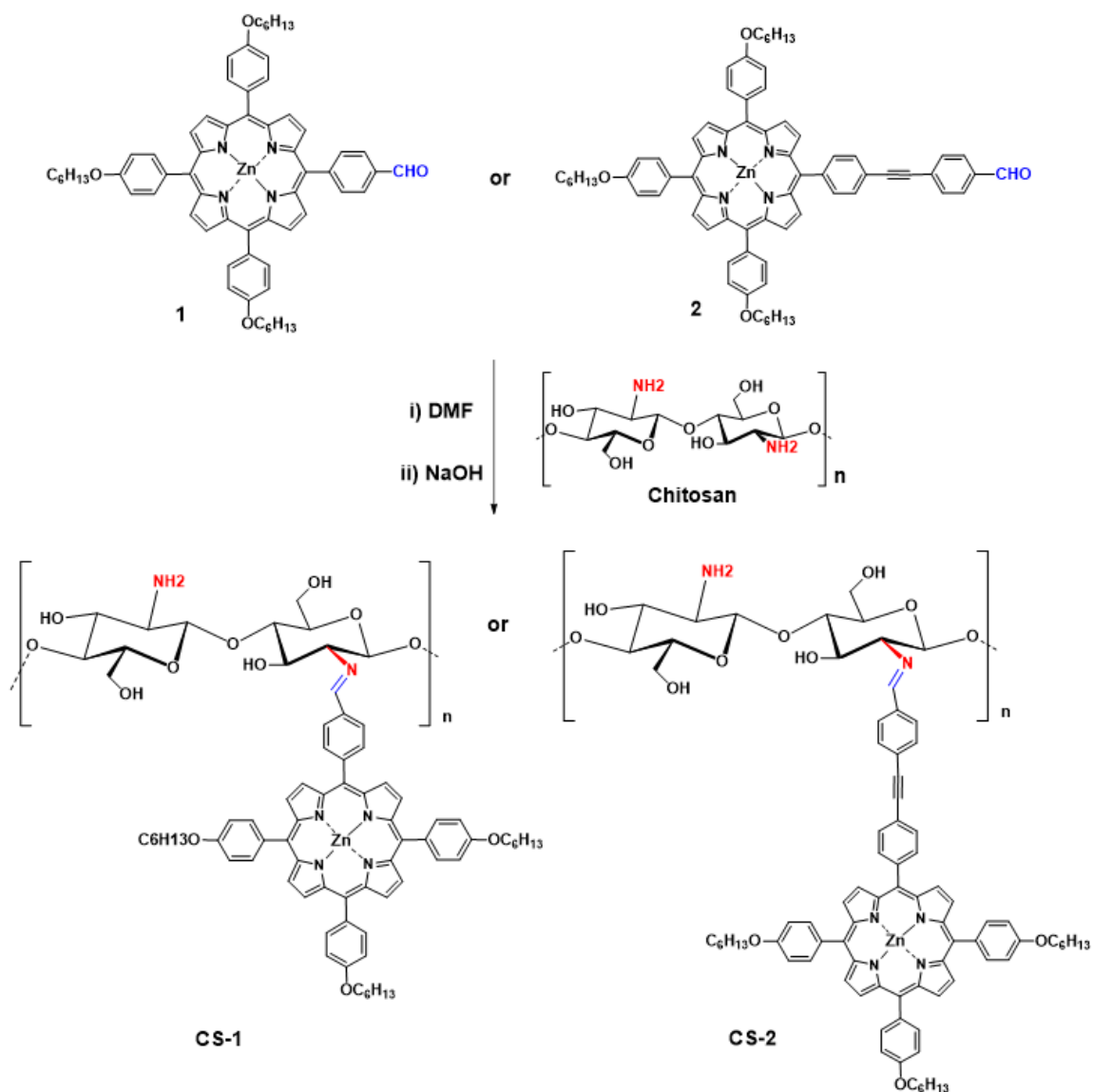
For porphyrin and chitosan conjugation, previously reported methods were used with slight modifications [22, 29-32]. Briefly mixing chitosan in 1% acetic acid solution with Zn(II) porphyrin in DMF at a 10 wt% concentration resulted in covalently linked hydrogel formation. To confirm the successful synthesis of chitosan hydrogels, FT-IR, UV-vis and SEM spectroscopic methods were applied. The FT-IR spectra of aldehyde substituted Zinc(II) porphyrins 1 and 2 exhibit a distinctive sharp and intense peak at 1723 cm^{-1} for the $C=O$, and for the aldehydic $C-H$ stretching absorptions at 2856 cm^{-1} and 2852 cm^{-1} respectively, characteristic of aldehyde vibration (Figure 1-2). Figure S7 represents the FT-IR spectrum of non-conjugated commercial chitosan. Two characteristic peaks at 3361 cm^{-1} and 3285 cm^{-1} that correspond to $-NH$ and $-OH$ functional groups of chitosan. Also $-N-H$ bending vibration of primary amine ($-NH_2$) of chitosan appears at 1574 cm^{-1} [39]. $-C-O-C$ stretching vibrations at 1061 cm^{-1} and symmetrical vibration of the $-C-O-H$ at 1024 cm^{-1} are known as fingerprint peaks of chitosan in the FT-IR spectra [40]. The bands at 1149 cm^{-1} and 894 cm^{-1} are representing the typical of the chitosan β glycosidic bond [41]. In the FT-IR spectra of the CS-1 and CS-2 the absorption band specific to the symmetric vibration $C=O$ of porphyrin at 1723 cm^{-1} fully disappeared in the spectrum of dried hydrogel, confirming that porphyrin attached to chitosan via imine bonds while a new peak of $C=N$ at 1649 cm^{-1} appeared

more intense than chitosan on this curve, confirming the reaction between chitosan and aldehyde groups on porphyrins as linkers (Figure 1-2).

Morphology of Chitosan Hydrogel

As mentioned earlier, hydrogels have been widely employed as frameworks owing to their outstanding biological performance, inherent ability for cellular interaction, and resemblance to the extracellular matrix. The morphology, including factors such as porosity and pore structure of the scaffold, plays a crucial role in influencing the diffusion of nutrients or oxygen, mec-

hanical properties, and the growth of cells within the three-dimensional structure of hydrogels [42]. After the CS-Por hydrogels were sampled, and dried on a grid, the internal morphology of them was investigated by scanning electron microscopy (SEM), as shown in Figure 3. Porphyrin-containing hydrogels CS-1 and CS-2 showed uniform coloration indicating homogeneous distribution of the dye over the entire material. CS-1 and CS-2 displayed a purple-green color consistent with the dispersed dye species, while the pure chitosan hydrogel without porphyrins tended to be colorless as expected (Figure 3). SEM images of the porphyrin-conjugated chi-



Scheme 1. Synthesis of porphyrin-conjugated chitosan hydrogel CS-1 and CS-2.

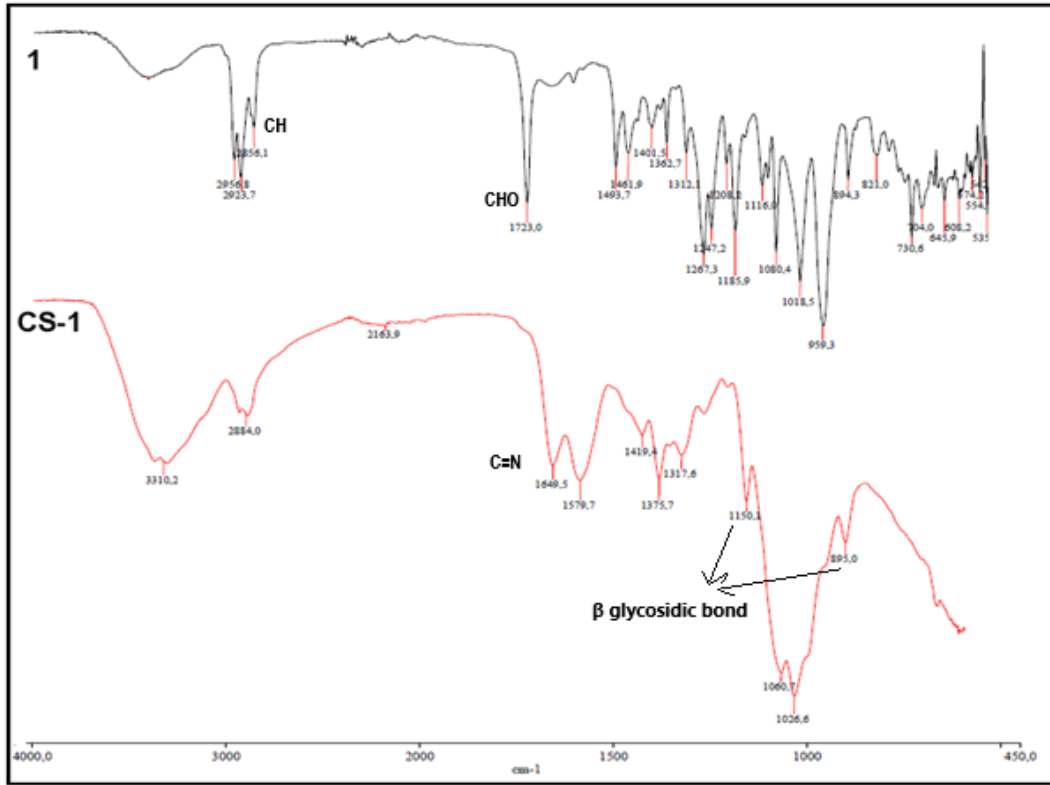


Figure 1. FT-IR spectra of Zn(II) Porphyrin 1 and chitosan hydrogel CS-1.

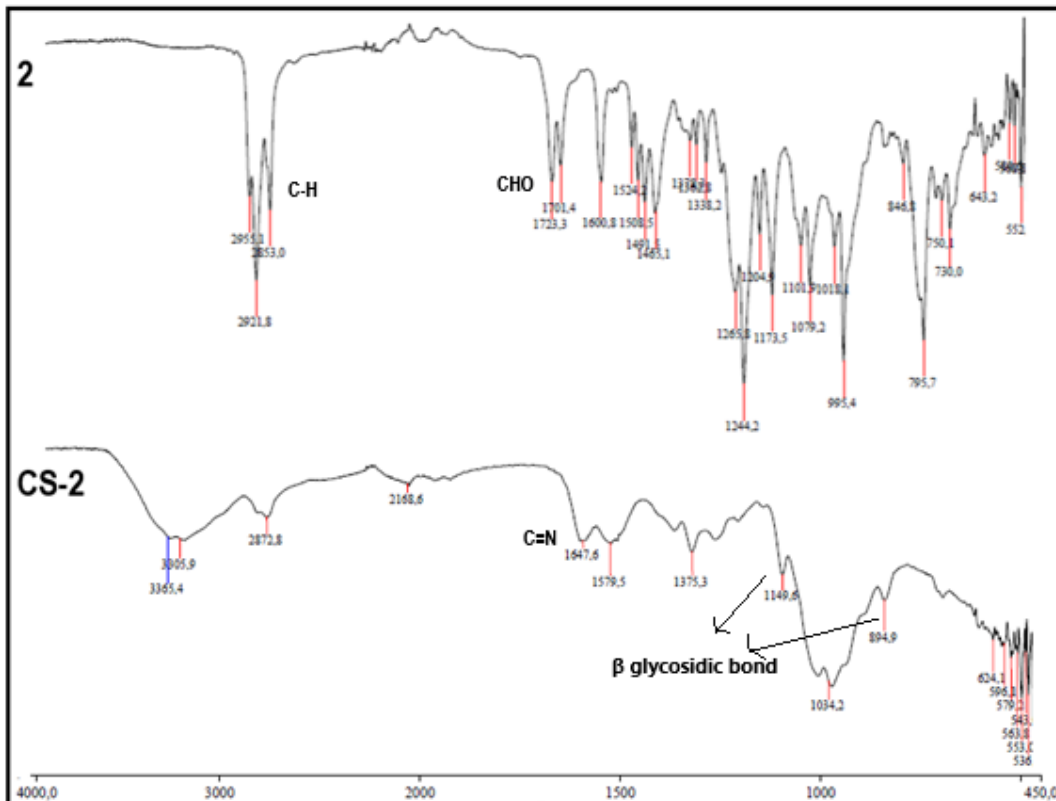


Figure 2. FT-IR spectra of Zn(II) Porphyrin 2 and chitosan hydrogel CS-2.

tosan further confirm their homogeneous distribution and morphology within the hydrogel matrix.

Photophysical and Photochemical Properties

Photochemical (singlet oxygen generation) properties of Zinc(II) porphyrins 1, 2, and porphyrin- conjugated chitosan hydrogel CS-1 and CS-1 were investigated in comparison with unsubstituted tetraphenyl porphyrin (TPP) in DMSO. DMSO served as the solvent owing to its non-toxic properties in biological environments. All of the data discussed below are summarized in Table 1.

Ground State Absorption

Porphyrins show a strong UV-visible absorption peak, known as the Soret band, near 400 nm, and a weaker Q band near 550 nm. These bands, caused by electron transitions between molecular orbitals, are key to understanding porphyrins' photochemical properties [43]. The behavior of metalloporphyrins in ground state absorption undergoes changes upon metal insertion, leading to a collapse of the Q band region from four bands to two. This alteration is attributed to an increase in symmetry (TPP, D_{2h} ; ZnTPP, D_{4h}) within the porphyrin macrocycles[44-46].

The optical characteristics of porphyrins and chitosan

hydrogels were evaluated by analyzing UV-vis spectra of 10 μM solutions in DMSO (Figure 4). All structures followed the Lambert–Beer law, revealing a consistent linear relationship between absorbance and concentrations in DMSO throughout the entire concentration measurement range. Complexes 1 and 2 exhibited the Soret bands at 431 and 432 nm respectively and relatively weak Q bands in the 564–608 nm region (Figure 5A and 5B). Both complexes display absorption at nearly identical wavelengths, suggesting that, contrary to complex 1, the incorporation of a second benzene ring as a spacer, connected to the *meso*-phenyl group in complex 2 via a triple bond did not yield the anticipated impact on conjugation.

To evaluate the optical properties of porphyrin conjugate chitosan hydrogels, 10 μM solutions in DMSO were formulated by dissolving completely dried hydrogels containing 10 wt% porphyrin. To achieve this, 0.220 mg of CS-1 (with 0.02 μM porphyrin) and 0.242 mg of CS-2 (with 0.02 μM porphyrin) hydrogels were individually weighed and dissolved in 2 mL of DMSO each. The absorption spectra of the Chitosan CS-1 and CS-2 hydrogels exhibited the same features as well as the porphyrin complexes 1 and 2 in DMSO, characterized by distinct Q-bands at the same wavelengths. (Figure 5C and

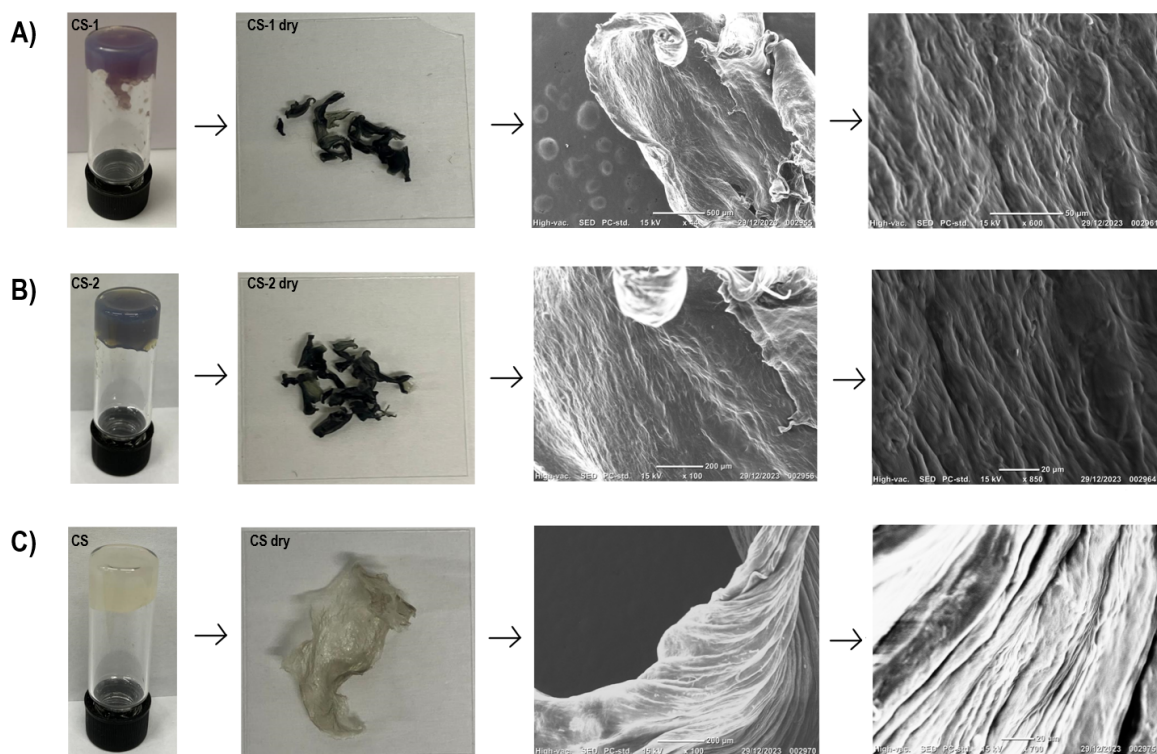


Figure 3. Pictures of hydrogels, dry form of hydrogels and SEM images of A) CS-1, B) CS-2 and C) non-conjugated CS.

5D). Additionally, no aggregation behavior was observed in the chitosan conjugates. These findings indicate that the photophysical characteristics of porphyrins remained largely unaltered following its conjugation with chitosan. Porphyrin 2 and its chitosan-conjugated derivative CS-2 showed the highest absorption intensity in DMSO (Table 1) among all compounds. It can be expected that the presence of a phenylacetylene unit acting as a spacer group on porphyrin effectively prevented aggregation. Table 1 summarizes the wavelengths and associated extinction coefficients in Soret-band, Q_{01} , and Q_{00} bands.

Singlet Oxygen Quantum Yields (Φ_{Δ})

Singlet oxygen quantum yield represents the ratio of the number of singlet oxygen molecules produced to the number of absorbed photons. The Φ_{Δ} value provides valuable insights into the effectiveness of a photosensitizer in generating singlet oxygen, which is a key reactive oxygen species involved in various photochemical and photophysical processes [47]. Various methods have been developed over the past five decades to measure the efficiency of Φ_{Δ} [48-50]. Indirect methods, such as chemical trapping and O_2 consumption techniques [51,52] are applicable in both organic and aqueous environments. In this study, the determination of Φ_{Δ} values was carried out using an indirect method in

DMSO. DMSO is a solvent commonly employed as a penetration enhancer in clinical settings to facilitate drug delivery into tissues [53]. It is essential to acknowledge that although DMSO serves as an appropriate solvent for these investigations, it does not mimic the complexities of biological environments, but these measurements are performed to assess whether the conjugation to chitosan affects or not the intrinsic photoproperties of the porphyrins. In this study, as an indirect method, measurements involved monitoring the disappearance of the absorption band of 1,3-diphenylisobenzofuran (DPBF) during irradiation, with subsequent monitoring of the quenching by the singlet oxygen generated using UV-Vis spectroscopy. Figure 6A-D depict the absorbance intensity of DPBF (at 417 nm) when exposed to porphyrin complexes 1 and 2, as well as porphyrin-conjugated hydrogels CS-1 and CS-2, respectively, over time with irradiation.

The literature contains substantial research on porphyrin-chitosan conjugates for efficient singlet oxygen generation, enabled when the photosensitizer's triplet state becomes populated, facilitating reactions with molecular oxygen. For example, Ferreira et al. developed six distinct film types for evaluating photodynamic therapy (PDT) efficiency, including chitosan-only and chitosan-porphyrin combinations, with singlet oxygen

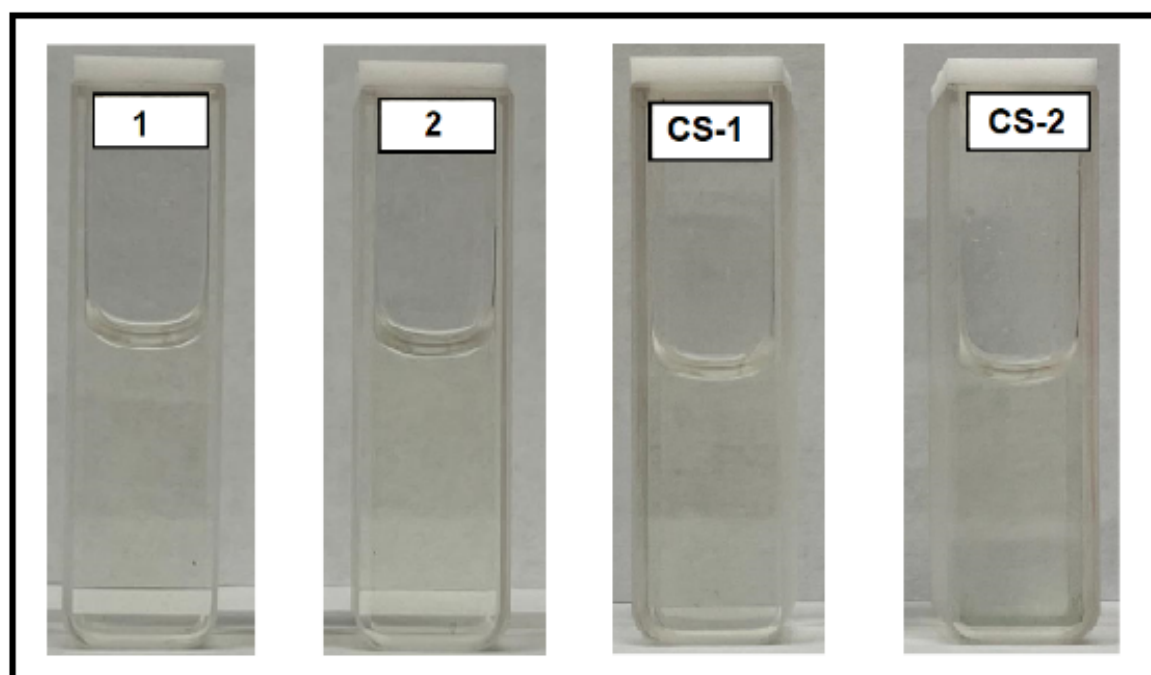


Figure 4. 10 μ M solutions of 1, 2, CS-1, CS-2 in DMSO respectively.

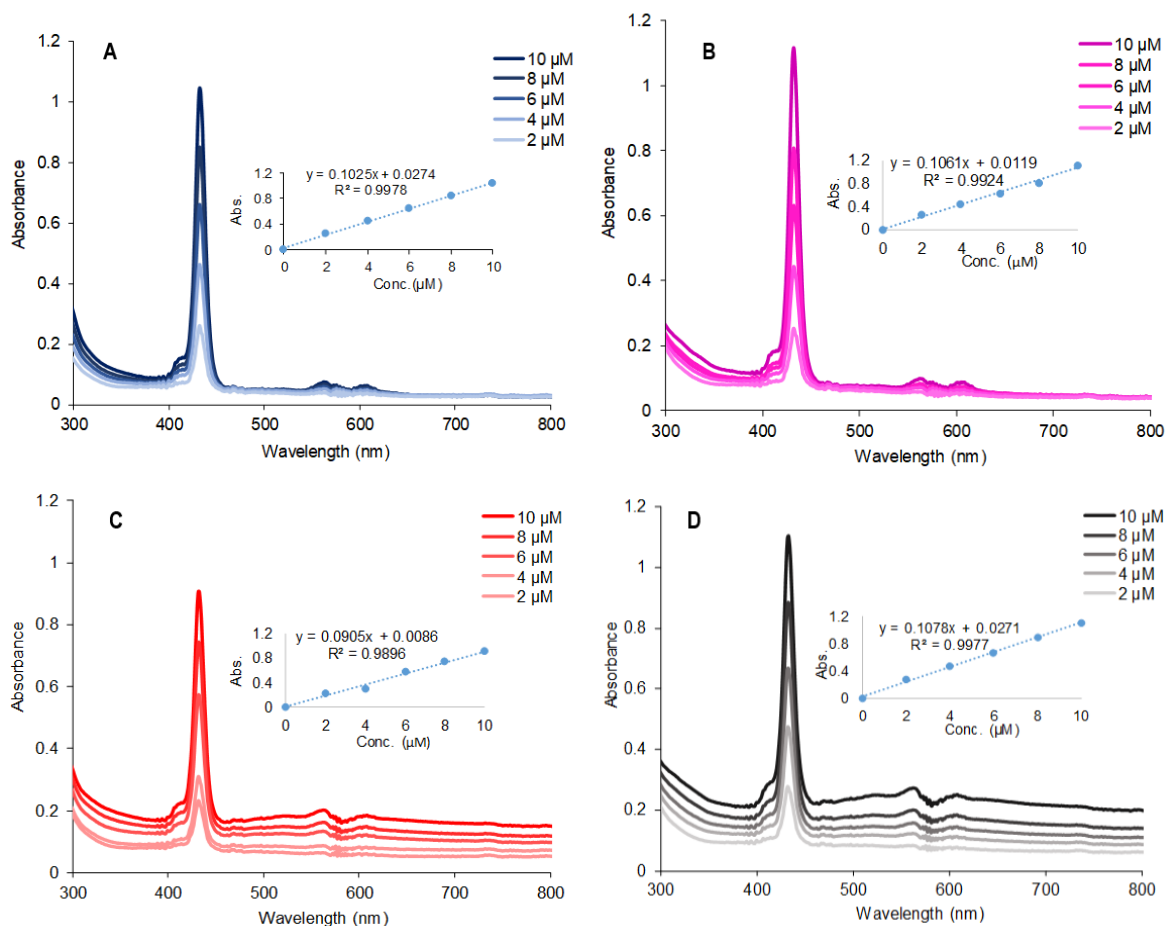


Figure 5. UV-vis absorption spectra of A) 1), B) 2), C) CS-1 and D) CS-2 in DMSO solutions of 2-10 μM concentration range. Insets: absorbance vs. concentration.

quantum yields around 50% [54]. Similarly, Li et al. observed comparable results by integrating porphyrin-based carbon dots (TPP CDs) with chitosan, where a significant reduction in DPBF absorption (50%) after 28 minutes of irradiation indicated reactive oxygen species (ROS) generation [55].

Belali et al. developed a CS/ NH_2 -TPP/FA hydrogel as a photosensitizer carrier for selective PDT, achieving a singlet oxygen delivery efficiency of 0.64 [27]. Castrol et al. reported the synthesis of cationic porphyrin-chitosan conjugates for antimicrobial PDT (aPDT), where DPiBF decay indicated efficient singlet oxygen production under the tested conditions [25].

Zhang et al. constructed an antimicrobial system utilizing chitosan-encapsulated metal-organic nanoparticles (Fe-TCPP@CS NPs) with TCPP as a photosensitizer, facilitating both photodynamic and photothermal

therapies. The porphyrins within these nanoparticles effectively transferred energy to molecular oxygen to generate singlet oxygen [56].

Another example includes 5,10,15,20-tetrakis(pentafluorophenyl)porphyrin [H2(TPFPP)] immobilized within chitosan to form hybrid nanoparticles for PDT, achieving a singlet oxygen quantum yield of 0.69 without compromising photophysical properties [24]. Furthermore, Sen et al. demonstrated that hybrid structures of cationic palladium porphyrins with chitosan significantly enhance singlet oxygen generation (SOG), achieving Φ_{Δ} values between 0.51 and 0.66 [57].

Recent studies indicate that among chitosan-conjugated macrocycle derivatives, structures incorporating chlorin e6 (Ce6) and phthalocyanine (Pc) have achieved the most effective results, demonstrating notably high singlet oxygen yields. For instance, Zhang et al. repor-

ted a chitosan-Ce6 nano-assembly with $^1\text{O}_2$ generation reaching up to 80% [58], while Stokov et al. achieved an SOG efficacy of 0.89 for chitosan-SiPc conjugates, significantly surpassing that of SiPc alone ($\Phi_{\Delta} = 0.44$) [31].

In our study, comparing the singlet oxygen quantum yields (Φ_{Δ}) among the porphyrin complexes, complex 1 exhibits a SOG of 50%, while complex 2 demonstrates a higher SOG of 68%. Structurally, the presence of the phenylacetylene group as a spacer leads to the increase in SOG generation. This spacer group effect persists when transitioning to hydrogel structures formed through porphyrin chitosan conjugation. The Φ_{Δ} value of CS-2 (78%) surpasses that of CS-1 (52%). Consequently, when considering all structures collectively, porphyrin-conjugated hydrogels demonstrate superior singlet oxygen generation compared to non-conjugated porphyrins at equivalent concentrations. These findings highlight the effectiveness of the hydrogel structure in enhancing the singlet oxygen generation of porphyrins. The network within the hydrogel structure proves to be a valuable system for preventing the self-quenching of porphyrins, thereby enabling effective singlet oxygen generation. In comparison to the existing literature, the CS-2 hydrogel developed in our study demonstrates the highest singlet oxygen generation efficiency ($\Phi_{\Delta} = 78\%$) among reported chitosan-conjugated porphyrin hydrogels. This highlights the efficacy of our approach in enhancing photodynamic activity through optimized chitosan-porphyrin conjugation.

In the sono-photochemical investigations, porphyrins 1, 2, and chitosan hydrogels CS-1 and CS-2 were subjected to simultaneous ultrasound and light irradiation for 10 seconds (initially 5 seconds of ultrasound followed by 5 seconds of light). The observed changes are depicted in Figure 7A-D. The calculated Φ_{Δ} values for compounds 1, 2, and chitosan hydrogels CS-1 and CS-2 are outlined in Table 1. For this sono-photodynamic therapy (SPDT) application, a 35 kHz ultrasound frequency was selected to evaluate the influence of ultrasound irradiation on the singlet oxygen production capacities of the investigated photosensitizing candidates, employing consistent UV-vis spectra [59], in contrast to the conventional ultrasound frequency used in standard literature studies (around 1 MHz) [60,61]. In sono-photodynamic studies, the singlet oxygen generation further increased to 0.56, 0.76, 0.58, and 0.81 for compounds 1, 2, and chitosan hydrogels CS-1 and CS-2 respectively, rep-

resenting approximately 10% improvement compared to photodynamic studies. Among all compounds the highest singlet oxygen quantum yield Φ_{Δ} value of 81% of CS-2, attributed to the presence of the spacer group and chitosan conjugation. For PDT or SPDT applications, when the sono-photochemical studies of well-known photosensitizers such as porphyrins and phthalocyanines which are the synthetic analogs of the naturally-existing porphyrins and their composite structures in the literature are examined, it is seen that the studies on phthalocyanines [62-67] have increased in the last 5 years. However, the same increase has not been seen for porphyrin macrostructures and their conjugate derivatives [68-72]. This study aims to fill the gap in the field of sono-photochemical studies of porphyrin structures. It is also important as it is the first sono-photochemical study of porphyrin-conjugated chitosan hydrogels. Moreover, considering the singlet oxygen generation value (Φ_{Δ}), which is the most important parameter in PDT and SPDT methods, both photochemical and sono-photochemical studies in this research showed that porphyrins 1 and 2 and their conjugated chitosan hydrogel forms have similar or higher values than the reference TPP value ($\Phi_{\Delta} = 0.52$). These findings highlight the effective enhancement of singlet oxygen quantum yield achieved by both the designed compounds and the applied method. Hence, whether or not sono-photodynamic therapy (SPDT) is applied, the successful generation of singlet oxygen from hydrogels confirms the potential of this system as a promising candidate for crafting a novel system aimed at eliminating cancer cells through the PDT or SPDT method.

Photodegradation Quantum Yield (Φ_d)

Photodegradation involves the oxidative decomposition of the photosensitizer when exposed to light irradiation, and this process is assessed through quantum efficiency. In photodynamic therapy (PDT), the photodegradation quantum yield (Φ_d) of the photosensitizer holds a crucial significance. The Φ_d value indicates the compound's stability under light irradiation. Examining the quantum yield of photodegradation offers valuable insights into the efficiency of porphyrins in producing reactive oxygen species (ROS) and their capacity to induce the targeted degradation of specific biomolecules. According to the literature, the quantum yield of photodegradation (Φ_d) for stable photosensitizers typically falls within the range of 10^{-3} to 10^{-6} [73]. In this study, the photodegradation of the compounds in DMSO was examined after exposure to light at 10-minute intervals

by monitoring the reduction in absorbance. Figure 8A-D illustrate the changes in the Q band of the compounds. The photodegradation quantum yield (Φ_d) values of the studied compounds 1, 2, CS-1, and CS-2 in DMSO are given in Table 1. The Q band intensity of the compounds remained unchanged in DMSO under light irradiation. All investigated porphyrin structures and chitosan hydrogel derivatives exhibited comparable stability, with a Φ_d on the order of 10^{-4} . This range demonstrates a relatively stable behavior under irradiation, with minimal reductions in Q band absorbance over the light exposure intervals.

Comparing these findings with existing literature highlights several insights into the stability of these porphyrin structures. For instance, the Golec et al have studied on free base and zinc porphyrins observed increased Φ_{pb} in deoxygenated solutions due to prolonged triplet state lifetimes, which led to faster photodecomposition and lower stability under similar conditions [74]. In

contrast, our current findings in DMSO suggest that the chitosan conjugation of porphyrins CS-1 and CS-2 not only maintains photostability but also effectively stabilizes the porphyrin core, with Φ_d values lower than observed in their study for unbound forms.

Additionally, Castro et al reported on cationic porphyrins bound to chitosan, the Φ_{pb} values for immobilized porphyrins also remained lower than their unbound counterparts, suggesting that the chitosan matrix effectively mitigates photodegradation by physically limiting the porphyrin's molecular freedom and exposure to ROS. This stability enhancement is beneficial for prolonged ROS generation, especially in PDT applications, where controlled ROS production without excessive degradation is desired for efficient bacterial inactivation [25].

Lastly, the study on hematoporphyrin-carboxymethyl chitosan nanoparticles showed that the aggregation-

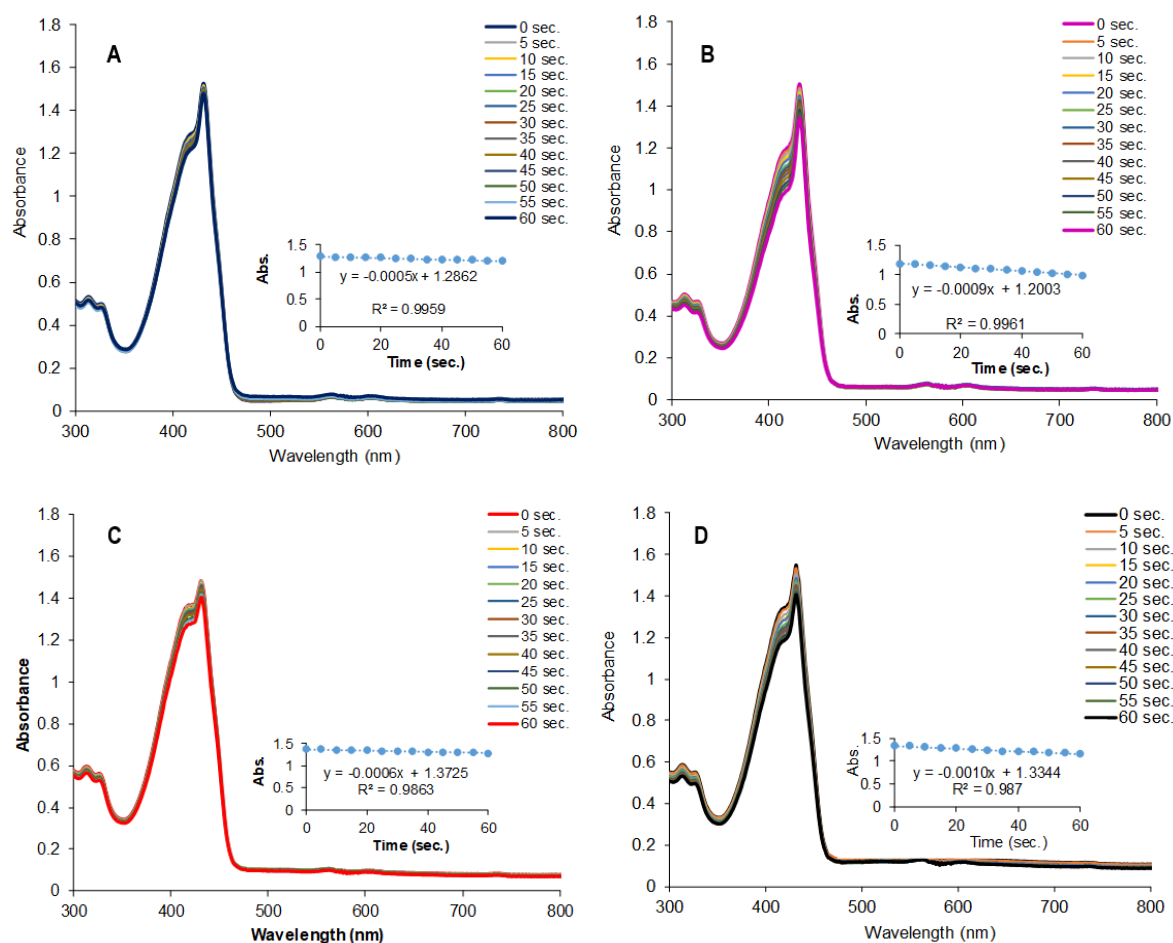


Figure 6. Determination of singlet oxygen quantum yield of A) 1, B) 2, C) CS-1 and D) CS-2 in DMSO, respectively. Inset: Plot of DPBF absorbance at 417 nm vs. time.

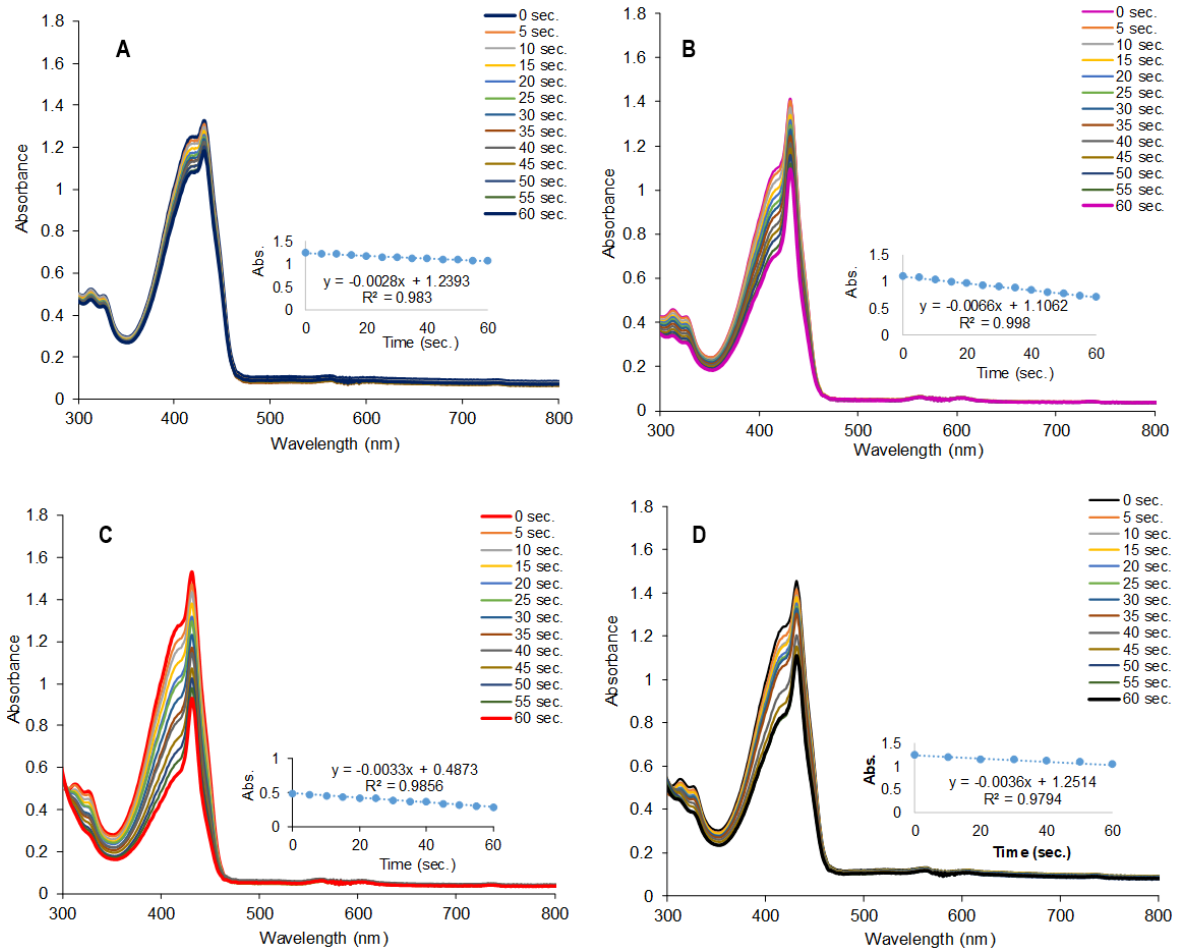


Figure 7. Determination of singlet oxygen quantum yield of A) 1, B) 2, C) CS-1 and D) CS-2 in DMSO by sono-photochemical process, respectively. Inset: Plot of DPBF absorbance at 417 nm vs time.

caused quenching effect in such systems significantly reduced Φ_d , boosting both photostability and ROS efficacy under light exposure [75]. Consistent with this finding, our chitosan-porphyrin conjugates (CS-1 and CS-2) exhibit enhanced stability and comparable Φ_d values, which reinforce the beneficial role of chitosan in preserving porphyrin's photodynamic functionality.

In conclusion, our results demonstrate that both free and chitosan-bound porphyrins maintain relatively low photodegradation quantum yields in DMSO, with chitosan conjugation enhancing stability. These findings align with the literature, where chitosan matrices consistently reduce photodegradation rates, supporting the suitability of chitosan-bound porphyrins as stable photosensitizers for extended use in applications requiring controlled ROS production, such as photodynamic therapy.

Conclusion

This study presents a novel approach to enhance the singlet oxygen generation efficiency of porphyrins by covalently conjugating them to chitosan hydrogel matrices. The successful covalent linkage of porphyrins to chitosan hydrogels was confirmed using spectroscopic and microscopic techniques. Photochemical studies revealed that the hydrogel structures exhibited superior singlet oxygen generation compared to free porphyrins in solution, with the presence of a phenylacetylene spacer further enhancing singlet oxygen production. Sono-photochemical investigations demonstrated the potential of these hydrogels for enhanced singlet oxygen generation under ultrasound and light irradiation. Moreover, the stability of the synthesized compounds under light irradiation suggests their suitability for PDT and SPDT applications. Overall, the results suggest that porphyrin-chitosan hydrogels hold promise as effective photosensitizers for PDT and SPDT applications, offering

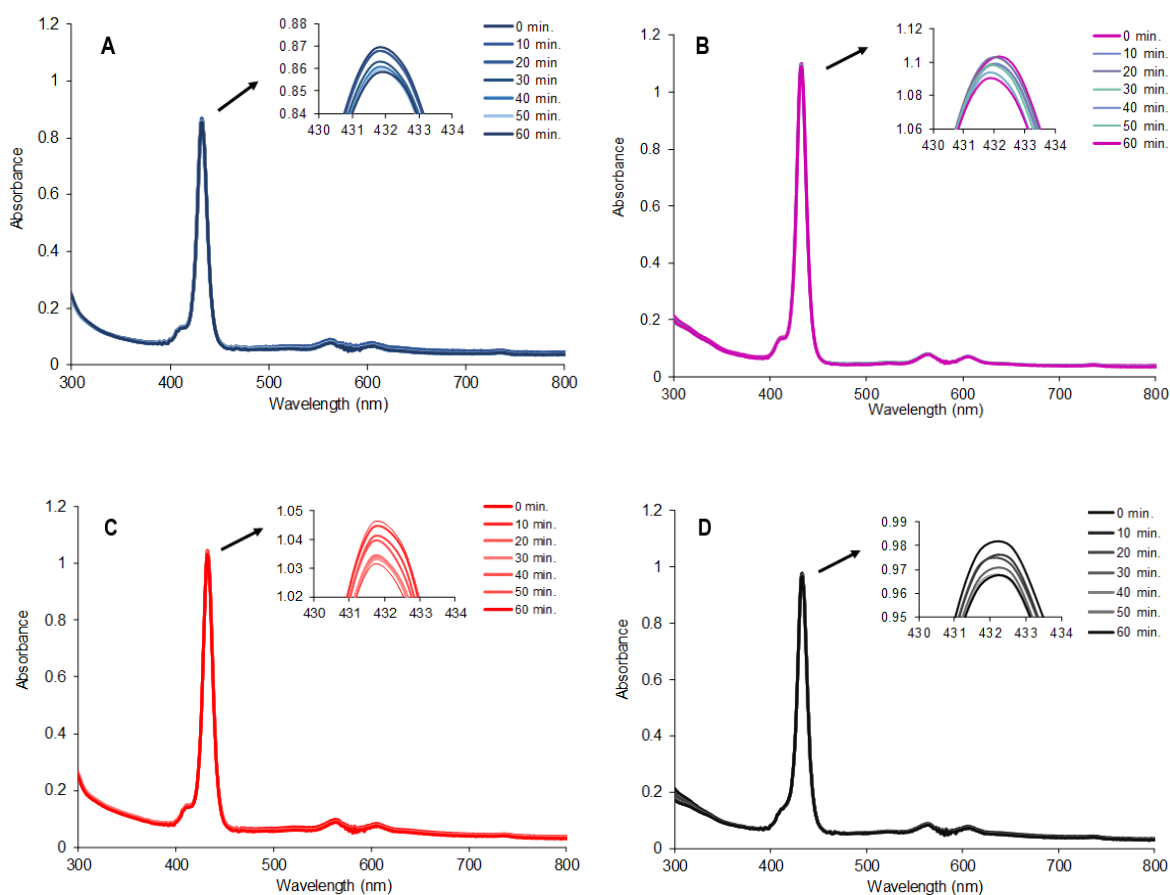


Figure 8. UV-Vis spectral change of A) 1, B) 2, C) CS-1 and D) CS-2 during photodegradation measurements in DMSO, respectively.

Table 1. Photophysical and photochemical properties of 1, 2, CS-1 and CS-2 in DMSO.

Compound	Soret (log ϵ)	$Q_y(1,0)$	$Q_y(0,0)$	$Q_x(1,0)$	Φ_{Δ}	$S\Phi_{\Delta}$	Φ_d
1	432 (5.01)	564 (3.83)	607 (3.74)	-	50	56	1.14×10^{-4}
2	432(5.04)	565 (3.89),	608 (3.85)	-	68	76	3.50×10^{-4}
CS-1	432(4.95)	566 (4.26),	609 (4.22)	-	52	58	2.13×10^{-4}
CS-2	432(5.03)	566 (4.39),	609 (4.35)	-	78	81	2.08×10^{-4}
H ₂ TPP	419 (5.6)	516 (4.33)	548 (4.19)	589 (4.09)	0.5276	-	-

improved biocompatibility, stability, and singlet oxygen generation efficiency compared to non-conjugated porphyrins. These results highlight the versatility and effectiveness of porphyrin-conjugated chitosan hydrogels as agents for targeted cancer therapy, emphasizing the need for additional research into their therapeutic applications and potential clinical use. Further investigations are necessary to assess the therapeutic efficacy of these hydrogels in both in vitro and in vivo models of cancer and other diseases.

Supplementary materials

FT-IR spectrum of non-conjugated chitosan, Mass spectra and ¹H NMR spectra, ¹³C NMR spectra of porphyrins 1 and 2 are given in the supplementary material.

References

1. D. Aebisher, P. Woźnicki, D. Bartusik-Aebisher, Photodynamic Therapy and Adaptive Immunity Induced by Reactive Oxygen Species: Recent Reports. *Cancers*, 16 (2024) 967.
2. L. Serpe, F. Giuntini, Sonodynamic antimicrobial chemotherapy: First steps towards a sound approach for microbe inactivation, *J. Photochem. Photobiol. B: Biol.*, 150 (2015) 44-49.
3. V. Choi, M.A. Rajora, G. Zheng, Activating Drugs with Sound: Mechanisms Behind Sonodynamic Therapy and the Role of Nanomedicine, *Bioconjugate Chem.*, 31 (2020) 967-989.
4. Y. Zheng, J. Ye, Z. Li, H. Chen, Y. Gao, Recent progress in sono-photodynamic cancer therapy: From developed new sensitizers to nanotechnology-based efficacy-enhancing strategies, *Acta Pharmacol. Sin.*, 11 (2021) 2197-2219.
5. S. Li, Q. Zou, Y. Li, C. Yuan, R. Xing, X. Yan, Smart Peptide-Based Supramolecular Photodynamic Metallo-Nanodrugs Designed by Multicomponent Coordination Self Assembly, *J. Am. Chem. Soc.*, 140 (2018) 10794-10802.
6. W. Wei, Z.X. Zhao, B.H. Xia, W. Li, Theoretical analysis of expanded porphyrins: Aromaticity, stability, and optoelectronic properties, *Front. Chem.*, 10 (2022) 1-10.
7. P. Henke, J. Dolanský, P. Kubát, J. Mosinger, Multifunctional Photosensitizing and Biotinylated Polystyrene Nanofiber Membranes/Composites for Binding of Biologically Active Compounds, *ACS Appl. Mater.*, 12 (2020) 18792-18802.
8. W. Yu, Z. Zhen, Q. Zhang, Y. Li, H. Luo, J. He, Y.M. Liu, Porphyrin-Based Metal-Organic Frameworks compounds as a promising nanomedicine in photodynamic therapy, *ChemMedChem.*, 15 (2020) 1766-1775.
9. P. Pallavi, K. Harini, V.A. Arumugam, P. Gowtham, K. Girigoswami, S. Muthukrishnan, A. Girigoswami, Nanoformulation of Tetrapyrroles Derivatives in Photodynamic Therapy: A Focus on Bacteriochlorin, *Evid.-Based Complementary Altern. Med.*, (2022) 1-12.
10. L. Shi, C. Nguyen, M. Daurat, N. Richey, C. Gauthier, E. Rebec, M. Gary-Bobo, S. Cammas-Marion, O. Mongin, C.O. Paul-Roth, F. Paul, Encapsulation of Hydrophobic Porphyrins into Biocompatible Nanoparticles: An Easy Way to Benefit of Their Two-Photon Phototherapeutic Effect without Hydrophilic Functionalization, *Cancers*, 14 (2022) 2358.
11. A. Garcia-Sampedro, A. Tabero, I. Mahamed, P. Acedo, Multimodal use of the porphyrin TMPyP: From cancer therapy to antimicrobial applications, *Porphyrin Science by Women 3*, (2021) 11-27.
12. N. Rabiee, M.T. Yarak, S.M. Garakani, S. Ahmadi, A. Lajevardi, M. Bagherzadeh, M. Rabiee, L. Tayebi, M. Tahriri, M.R. Hamblin, Recent Advances in Porphyrin-Based Nanocomposites for Effective Targeted Imaging and Therapy, *Biomaterials*, 232 (2020) 119707.
13. H.B. Cheng, B. Qiao, H. Li, J. Cao, Y. Luo, K.M.K. Swamy, J. Zhao, Z. Wang, J.Y. Lee, X.J. Liang, J. Yoon. Protein-Activatable Diarylethene Monomer as a Smart Trigger of Noninvasive Control Over Reversible Generation of Singlet Oxygen: A Facile, Switchable, Theranostic Strategy for Photodynamic-Immunotherapy. *J. Am. Chem. Soc.*, 143 (2021) 2413-2422.
14. V.S. Tyurin, A.O. Shkirdova, O.I. Koifman, I.A. Zamilatskov, Meso-Formyl, Vinyl, and Ethynyl Porphyrins—Multipotent Synthons for Obtaining a Diverse Array of Functional Derivatives, *Molecules*, 28 (2023) 5782.
15. W.H. Yin, P.Y. Li, H.H. Huang, L. Feng, S.H. Liu, X. Liu, F.Q. Bai, Porphyrin photosensitizer molecules as effective medicine candidates for photodynamic therapy: electronic structure information aided design, *RSC Adv.*, 14 (2024) 29368-29383.
16. E. Molnar, E. Gal, C. Cristea, L. Silaghi-Dumitrescu, Ethyne Functionalized Meso-Phenothiazinyl-Phenyl- Porphyrins: Synthesis and Optical Properties of Free Base Versus Protonated Species, *Molecules*, 225 (2020) 4546.
17. D.G. Kim, Y.I. Jeong, J.W. Nah, All-Trans Retinoic Acid Release from Polyion-Complex Micelles of Methoxy Poly(ethylene glycol) Grafted Chitosan, *J. Appl. Polym. Sci.*, 105 (2007) 3246-3254.
18. J.P. Nam, C. Choi, M.K. Jang, Y.I. Jeong, J.W. Nah, S.H. Kim, Y. Park, Insulin-incorporated chitosan nanoparticles based on polyelectrolyte complex formation, *Macromol. Res.*, 18 (2010) 630-635.
19. C.W. Chung, C.H. Kim, K.H. Choi, J.J. Yoo, D.H. Kim, K.D. Chung, Y.I. Jeong, D.H. Kang. Effect of surfactant on 5-aminolevulinic acid uptake and PpIX generation in human cholangiocarcinoma cell, *Eur. J. Pharm. Biopharm.*, 80 (2012) 453-458.
20. K.D. Chunga, Y.I. Jeong, C.W. Chung, D.H. Kimb, D.H. Kang. Anti-tumor activity of all-trans retinoic acid-incorporated glycol chitosan nanoparticles against HuCC-T1 human cholangiocarcinoma cells, *Int. J. Pharm.*, 422 (2012) 454-461.
21. G.M.F. Calixto, S.R. Annunzio, F.D. Victorelli, M.L. Frade, P.S. Ferreira, M. Chorilli, C.R. Fontana, Chitosan-Based Drug Delivery Systems for Optimization of Photodynamic Therapy, *AAPS PharmSciTech.*, 20 (2019) 253.
22. N. Maldonado-Carmona, T.S. Ouk, M.J.F. Calvete, M.M. Pereira, N. Villandier, S. Leroy-Lhez, Conjugating biomaterials with photosensitizers: advances and perspectives for Photodynamic Antimicrobial Chemotherapy, *Photochem. Photobiol. Sci.*, 19 (2020) 445-461.
23. M.S. Hasanin, M. Abdelraof, M. Fikry, Y.M. Shaker, A.M.K. Sweed, M.O. Senge, Development of Antimicrobial Laser-Induced Photodynamic Therapy Based on Ethylcellulose/Chitosan Nanocomposite with 5,10,15,20-Tetrakis(m-Hydroxyphenyl) porphyrin, *Molecules*, 26 (2021) 3551.
24. L.B. Silva, K.A.D.F. Castro, C.E.A. Botteon, C.L.P. Oliveira, R.S. Silva, P.D. Marcato, Hybrid Nanoparticles as an Efficient Porphyrin Delivery System for Cancer Cells to Enhance Photodynamic Therapy, *Front. bioeng. Biotechnol.*, 9 (2021) 1-15.
25. K.A.D.F. Castro, N.M.M. Moura, F. Figueira, R.I. Ferreira, M.M.Q. Simões, J.A.S. Cavaleiro, M.A.F. Faustino, A.J.D. Silvestre, C.S.R. Freire, J.P.C. Tomé, Nakagaki S, Almeida A, Neves MGPMS, New Materials Based on Cationic Porphyrins Conjugated to Chitosan or Titanium Dioxide: Synthesis, Characterization and Antimicrobial Efficacy, *Int. J. Mol. Sci.*, 20 (2019) 2522.
26. K. Li, P. Berton, S.P. Kelley, R.D. Rogers, Singlet Oxygen Production and Tunable Optical Properties of Deacetylated Chitin-Porphyrin Cross-Linked Films, *Biomacromolecules*, 19 (2018) 3291.
27. S. Belali, A.R. Karimi, M. Hadizadeh, Cell-specific and pH-sensitive nanostructure hydrogel based on chitosan as a photosensitizer carrier for selective photodynamic therapy, *Int. J. Biol. Macromol.*, 110 (2018) 437-448.
28. E. Önal, S.Z. Topal, I. Fidan, S. Berber, F. Dumoulin, C. Hirel, Structure-Photoproperties Relationship Investigation of the Singlet Oxygen Formation in Porphyrin-Fullerene Dyads, *J. Fluoresc.*, 27 (2017) 1855-1869.

29. A.R. Karimi, A. Khodadadi, M. Hadizadeh, A nanoporous photosensitizing hydrogel based on chitosan cross-linked by zinc phthalocyanine: an injectable and pH-stimuli responsive system for effective cancer therapy, *RSC Adv.*, 6 (2016) 91445.
30. P. Mandal, J.S. Manna, D. Dasb, M.K. Mitra, Excitonic dynamics of Chlorophyll-a molecules in chitosan hydrogel scaffold, *Photochem. Photobiol. Sci.*, 14 (2015) 786.
31. K. Stokov, A. Galstyan, Chitosan-Silicon Phthalocyanine Conjugate as Effective Photo-Functional Hydrogel for Tracking and Killing of Bacteria, *Eur. J. Org. Chem.*, 47 (2020) 7327–7332.
32. Y. Zhong, L. Zhang, S. Sun, S. Zhou, Y. Ma, H. Hong, D. Yang, Sequential drug delivery by injectable macroporous hydrogels for combined photodynamic-chemotherapy, *J. Nanobiotechnol.*, 19 (2021) 333.
33. N. Gandra, A.T. Frank, O.L. Gendre, N. Sawwan, D. Aebisher, J.F. Liebman, K.N. Houk, A. Greer, R. Gao, Possible singlet oxygen generation from the photolysis of indigo dyes in methanol, DMSO, water, and ionic liquid, 1-butyl-3-methylimidazolium tetrafluoroborate, *Tetrahedron*, 62 (2006) 10771–10776.
34. M. Korinek, R. Dedic, A. Molnar, A. Svoboda, J. Hala, A comparison of photosensitizing properties of meso-tetraphenylporphyrin in acetone and in dimethylsulfoxide, *J. Mol. Struct.*, 3 (2005) 727–731.
35. E. Göransson, J. Boixel, C. Monnereau, E. Blart, Y. Pellegrin, H.C. Becker, Hammarström L, Odobel F, Photoinduced Electron Transfer in Zn(II)porphyrin-Bridge- Pt(II)acetylide complexes: Variation in Rate with Anchoring Group and Position of the Bridge, *Inorg. Chem.*, 49 (2010) 9823–9832.
36. A. Lembo, P. Tagliatesta, D.M. Gulri, M. Wielopolski, M. Nuccetelli, Porphyrin- β -Oligo-Ethynylphenylene-[60] Fullerene Triads: Synthesis and Electrochemical and Photophysical Characterization of the New Porphyrin-Oligo-PPE-[60]Fullerene Systems, *J. Phys. Chem. A*, 113 (2009) 1779–1793.
37. C.W. Craven, K.R. Reissmann, H.I. Chinn, Infrared Absorption Spectra of Porphyrins, *Anal. Chem.*, 24 (1952) 1214–1215.
38. N.B. Colthup, Spectra-Structure Correlations in the Infra-Red Region, *J. Opt. Soc. Am.*, 40 (1950) 397.
39. P.Y. Zhuang, Y.L. Li, L. Fan, J. Lin, Q.L. Hu, Modification of chitosan membrane with poly(vinyl alcohol) and biocompatibility evaluation, *Int. J. Biol. Macromol.*, 50 (2012) 658–663.
40. H. Staroszczyk, K. Sztuka, J. Wolska, A. Wojtasz-Pająk, I. Kołodziejaska, Interactions of fish gelatin and chitosan in uncrosslinked and crosslinked with EDC films: FT-IR study, *Spectrochim. Acta A Mol. Biomol. Spectrosc.*, 117 (2014) 707–712.
41. L. Wei, Y. Chen, W. Tan, Q. Li, G. Gu, F. Dong, Z. Guo, Synthesis, Characterization, and Antifungal Activity of Pyridine-Based Triple Quaternized Chitosan Derivatives, *Molecules*, 23 (2018) 2604.
42. E. Kolanthai, P.A. Sindu, D.K. Khajuria, S.C. Veerla, D. Kuppaswamy, L.H. Catalani, D.R. Mahapatra, Graphene Oxide-A Tool for the Preparation of Chemically Crosslinking Free Alginate–Chitosan–Collagen Scaffolds for Bone Tissue Engineering, *ACS Appl. Mater. Interfaces.*, 10 (2018) 12441–12452.
43. D.F. Marsh, M.L. Mink, Microscale Synthesis and Electronic Absorption Spectroscopy of Tetraphenylporphyrin H₂(TPP) and Metalloporphyrins ZnII(TPP) and Ni II (TPP), *J. Chem. Ed.*, 73 (1996) 1181.
44. J.W. Buchler, W. Kokisch, P.D. Smith, Cis, trans, and metal effects in transition metal porphyrins. In: *Novel Aspects. Structure and Bonding*, Springer, Berlin, Heidelberg, 1978.
45. M. Gouterman, *The Porphyrins Phys. Chem. Part A.*, Academic Press, New York, U.S.A, 1978.
46. N.C.M. Magdaong, M. Taniguchi, J.R. Diers, D.M. Niedzwiedzki, C. Kirmaier, J.S. Lindsey, D.F. Bocian, D. Holten, Photophysical Properties and Electronic Structure of Zinc(II) Porphyrins Bearing 0–4 meso-Phenyl Substituents: Zinc Porphine to Zinc Tetraphenylporphyrin (ZnTPP), *J. Phys. Chem. A*, 124 (2020) 7776–7794.
47. Y. Wang, Y. Lin, S. He, S. Wu, C. Yang, Singlet oxygen: Properties, generation, detection, and environmental applications, *J. Hazard. Mater.*, 461 (2024) 132538.
48. A.A. Gorman, I. Hamblett, C. Lambert, A.L. Prescott, M.A.J. Rodgers, H.M. Spence, Aromatic ketone-naphthalene systems as absolute standards for the triplet-sensitized formation of singlet oxygen, (1O₂), in organic and aqueous media. A time-resolved luminescence study, *J. Am. Chem. Soc.*, 109 (1987) 3091–3097.
49. M. Niedre, M.S. Patterson, B.C. Wilson, Direct Near-infrared Luminescence Detection of Singlet Oxygen Generated by Photodynamic Therapy in Cells In Vitro and Tissues In Vivo, *Photochem. Photobiol.*, 75 (2002) 382–391.
50. R. Schmidt, C. Tanielian, R. Dunsbach, C. Wolff, Phenalenone, a universal reference compound for the determination of quantum yields of singlet oxygen O₂(1 Δ g) sensitization, *J. Photochem. Photobiol. A Chem.*, 79 (1994) 11–17.
51. W. Spiller, H. Kliesch, D. Wöhrle, S. Hackbarth, B. Röder, G. Schnurpfeil, Singlet Oxygen Quantum Yields of Different Photosensitizers in Polar Solvents and Micellar Solutions, *J. Porphyr. Phthalocyanines*, 2 (1998) 145–158.
52. I. Kraljić, S.E. Mohsni, A New Method For The Detection of Singlet Oxygen in Aqueous Solutions, *J. Photochem. Photobiol.*, 28 (1978) 577–581.
53. A.C. Williams, B.W. Barry, Penetration enhancers, *Adv. Drug Deliv. Rev.*, 56 (2004) 603 – 618.
54. D.P. Ferreira, D.S. Conceição, R.C. Calhelha, T. Sousa, R. Socoteanu, I.C.F.R. Ferreira, L.F.V. Ferreira, Porphyrin dye into biopolymeric chitosan films for localized photodynamic therapy of cancer, *Carbohydr. Polym.*, 151 (2016) 160–171.
55. Y. Li, X. Zheng, X. Zhang, S. Liu, Q. Pei, M. Zheng, Z. Xie, Porphyrin-Based Carbon Dots for Photodynamic Therapy of Hepatoma, *Adv. Healthcare Mater.*, 6 (2016) 1600924.
56. Y. Zhang, J. Ma, D. Wang, C. Xu, S. Shang, J. Cheng, C. Bau, Y. Li, H. Tian, Fe-TCPP@CS Nanoparticles as Photodynamic and Photothermal Agent for Efficient Antimicrobial Therapy, *Biomater. Sci.*, 8 (2020) 6526–6532.
57. P. Sen, R. Soy, S. Mgidlana, J. Mack, T. Nyokong, Light-driven antimicrobial therapy of palladium porphyrins and their chitosan immobilization derivatives and their photophysical-chemical properties, *Dyes Pigments*, 2023 (2022) 110313.
58. R. Zhang, Y. Li, M. Zhou, C. Wang, P. Feng, W. Miao, H. Huang, Photodynamic Chitosan Nano-Assembly as a Potent Alternative Candidate for Combating Antibiotic-Resistant Bacteria, *ACS Appl. Mater. Interfaces.*, 11 (2019) 26711–26721.
59. G.Y. Atmaca, Investigation of singlet oxygen efficiency of di-axially substituted silicon phthalocyanine with sono-photochemical and photochemical studies, *Polyhedron*, 193 (2021) 114894.
60. Y. Liu, P. Wang, Q. Liu, X. Wang, Sinoporphyrin sodium triggered sono- photodynamic effects on breast cancer both in vitro and in vivo, *Ultrason. Sonochem.*, 32 (2016) 437–448.

61. H. Chen, X. Zhou, Y. Gao, B. Zheng, F. Tang, Recent progress in development of new sonosensitizers for sonodynamic cancer therapy, *Drug. Discov. Today*, 19 (2014) 502-509.
62. N. Farajzadeh, G. Yaşa Atmaca, A. Erdoğan, M. Burkut Koçak, Comparatively singlet oxygen efficiency by sono-photochemical and photochemical studies of new lutetium (III) phthalocyanines, *Dyes Pigments*, 190 (2021) 109325.
63. Farajzadeh, S. Özdemir, S. Gonca, G. Yaşa Atmaca, A. Erdoğan, Z. Altuntaş Bayır, M. Burkut Koçak, Photophysical and Biological Properties of New Phthalocyanines Bearing 4-(trifluoromethoxy)phenoxy and 2-(4-methylthiazol-5-yl)ethoxy Groups on Peripheral Positions, *J. Photochem. Photobiol.*, 98 (2022) 894–906.
64. A. Günsel, N. Mutlu, G. Yaşa Atmaca, H. Günsel, A.T. Bilgiçli, A. Erdoğan, M. Nilüfer Yarasir, Novel Graphene Oxide/ Zinc Phthalocyanine Composites Bearing 3-Chloro-4-Fluorophenoxy: Potential Usage for Sono/Photochemical Applications, *ChemistrySelect*, 8 (2023) 1-7.
65. K. Granados-Tavera, M. Zambrano-Angulo, N. Montenegro-Pohlhammer, G. Yaşa Atmaca, L. Sobotta, E. Güzel, G. Cardenas-Jiron, A. Erdoğan, A.G. Gürek, Synergistic effect of ultrasound and light to efficient singlet oxygen formation for photodynamic purposes, *Dyes Pigments*, 210 (2023) 110986.
66. A. Günsel, M.C. Küçük, H. Günsel, G. Yaşa Atmaca, A.T. Bilgiçli, A. Erdoğan, M. Nilüfer Yarasir, 3-Chloro-4-fluorophenoxy substituted zinc phthalocyanine/graphene oxide composites: exploring of their sono-photochemical properties, *Chem. Pap.*, 77 (2023) 5721–5731.
67. G. Yaşa Atmaca, K. Celep, A. Erdoğan, Application of comparative sonochemical, photochemical, and sono-photochemical methods to obtain new silicon phthalocyanine with high singlet oxygen efficiency, *J. Organomet. Chem.*, 1004 (2024) 122952.
68. Y. Yang, J. Tu, D. Yang, J.L. Raymond, R.A. Roy, D. Zhang, Photo- and Sono-dynamic therapy: A review of mechanisms and considerations for pharmacological agents used in therapy incorporating light and sound, *Curr. Pharm. Des.*, 25 (2019) 401-412.
69. K.A. Sadalana, P. Chaturvedi, Y.M. Seo, J.K. Kim, Y.S. Jo, Y.K. Lee, W.C. Ahn, Sono-Photodynamic Combination Therapy: A Review on Sensitizers, *Anticancer Res.*, 34 (2014) 457-4664.
70. M. Wysocki, B. Czarzynska-Goslinska, D. Ziental, M. Michalak, E. Güzel, L. Sobotta, Excited State and Reactive Oxygen Species against Cancer and Pathogens: A Review on Sonodynamic and Sono- Photodynamic Therapy, *ChemMedChem*, 17 (2022) 1-21.
71. S. Liao, M. Cai, R. Zhu, T. Fu, Y. Du, J. Kong, Y. Zhang, C. Qu, X. Dong, J. Ni, X. Yin, Antitumor Effect of Photodynamic Therapy/Sonodynamic Therapy/ Sono-Photodynamic Therapy of Chlorin e6 and Other Applications, *Mol. Pharmaceutics*, 20 (2023) 875–885.
72. M. Das, V. Pandey, K. Jajoria, D. Bhatia, I. Gupta, H. Shekhar, Glycosylated Porphyrin Derivatives for Sonodynamic Therapy: ROS Generation and Cytotoxicity Studies in Breast Cancer Cells. *ACS Omega*, 9 (2024) 1196–1205.
73. M. Durmus, Photochemical and photophysical characterization, Photosensitizers in medicine, environment, and security, Springer Dordrecht, 2011.
74. B. Golec, J. Buczyńska, K. Nawara, A. Gorski, J. Waluk, Photodegradation of free base and zinc porphyrins in the presence and absence of oxygen, *Photochem. Photobiol. Sci.*, 22 (2023) 2725–2734.
75. T. Zhou, Y. Yin, W. Cai, H. Wang, L. Fan, G. He, J. Zhang, M. Jiang, J. Liu, A new antibacterial nano-system based on hematoporphyrin-carboxymethyl chitosan conjugate for enhanced photostability and photodynamic activity, *Carbohydr. Polym.*, 269 (2021) 118242.
76. M. Taniguchia, J.S. Lindsey, D.F. Bocian, D. Holten, Comprehensive review of photophysical parameters (ϵ , ϕ_f , τ_s) of tetraphenylporphyrin (H2TPP) and zinc tetraphenylporphyrin (ZnTPP)-Critical benchmark molecules in photochemistry and photosynthesis, *J. Photochem. Photobiol. C: Photochem. Rev.*, 46 (2021) 100401.